JGR Solid Earth - A publication of AGU

C. M. Puskas
2007

JOURNAL OF GEOPHYSICAL RESEARCH, VOL. 112, B03401,
doi:10.1029/2006JB004325, 2007

Crustal deformation of the Yellowstone-Snake River Plain volcano-tectonic system: Campaign and continuous GPS observations, 1987-2004

C. M. Puskas and R. B. Smith
Department of Geology and Geophysics, University of Utah,
Salt Lake City, Utah, USA

C. M. Meertens
University NAVSTAR Consortium,
Boulder, Colorado, USA

W. L. Chang
Department of Geology and Geophysics, University of Utah,
Salt Lake City, Utah, USA

Abstract

[1] The Yellowstone–Snake River Plain tectonomagmatic province resulted from Late Tertiary volcanism in western North America, producing three large, caldera-forming eruptions at the Yellowstone Plateau in the last 2 Myr. To understand the kinematics and geodynamics of this volcanic system, the University of Utah conducted seven GPS campaigns at 140 sites between 1987 and 2003 and installed a network of 15 permanent stations. GPS deployments focused on the Yellowstone caldera, the Hebgen Lake and Teton faults, and the eastern Snake River Plain. The GPS data revealed periods of uplift and subsidence of the Yellowstone caldera at rates up to 15 mm/yr. From 1987 to 1995, the caldera subsided and contracted, implying volume loss. From 1995 to 2000, deformation shifted to inflation and extension northwest of the caldera. From 2000 to 2003, uplift continued to the

northwest while caldera subsidence was renewed. The GPS observations also revealed extension across the Hebgen Lake fault and fault-normal contraction across the Teton fault. Deformation rates of the Yellowstone caldera and Hebgen Lake fault were converted to equivalent total moment rates, which exceeded historic seismic moment release and late Quaternary fault slip-derived moment release by an order of magnitude. The Yellowstone caldera deformation trends were superimposed on regional southwest extension of the Yellowstone Plateau at up to 4.3 ± 0.2 mm/yr, while the eastern Snake River Plain moved southwest as a slower rate at 2.1 ± 0.2 mm/yr. This southwest extension of the Yellowstone–Snake River Plain system merged into east-west extension of the Basin-Range province.

Received 6 February 2006; revised 4 August 2006; accepted 6 October 2006; published 2 March 2007.

Keywords: Yellowstone hot spot, volcanic deformation, GPS measurements.

Index Terms: 8137 Tectonophysics: Hotspots, large igneous provinces, and flood basalt volcanism; 8178 Tectonophysics: Tectonics and magmatism; 8109 Tectonophysics: Continental tectonics: extensional (0905); 8419 Volcanology: Volcano monitoring (7280); 1240 Geodesy and Gravity: Satellite geodesy: results (6929, 7215, 7230, 7240).

---

1. Introduction

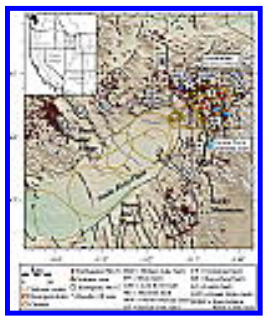

Figure 1. Index map of the Yellowstone–Snake River Plain magmatic-tectonic area showing earthquakes, Late Quaternary faults, and volcanic structures. Inset shows tectonic provinces of western United States and location of study area. Stars mark epicenters of significant historic earthquakes: (1) 1959 M7.5 Hebgen Lake, Montana, earthquake, (2) 1975 M6.1 Norris Junction, Wyoming, earthquake, (3) 1983 M7.3 Borah Peak, Idaho, earthquake, and (4) 1994 M5.9 Draney Peak, Idaho, earthquake. SRP rift zones associated with Holocene lava flows were obtained from *Kuntz et al.* [1986].

Figure 2. Map of campaign and continuous GPS stations in the YSRP used in this study. Continuous stations labeled separately. (left) Regional GPS network and (right) the Yellowstone National Park GPS network.

[2] The University of Utah (UU), in partnership with variously UNAVCO, the National Park Service, U.S. Geological Survey (USGS), Idaho National Laboratory, Brigham Young University, Massachusetts Institute of Technology, and the National Geodetic Survey conducted a series GPS studies of the Yellowstone–eastern Snake River Plain (YSRP) volcanic province of Idaho and Wyoming to understand the contemporary deformation associated with this continental hot spot and to assess its interaction with the extensional intraplate lithosphere (Figure 1). Campaign GPS surveys and a continuous GPS network measured deformation of the YSRP and surrounding tectonic areas (Figure 2).

[3] This study presents the results of over 16 years of campaign and 6 years of continuous GPS data acquisition and analysis. This paper is intended to serve as an archive of our data, processing, and interpretations of volcanic and tectonic deformation of the YSRP. Subsequent papers will concentrate on numerical modeling of the data, focusing on magmatic-hydrothermal sources, kinematics, and geodynamics of the YSRP in a western U.S. tectonic framework.

[4] We report deformation rates of the Yellowstone Plateau, which includes the 2 Ma Yellowstone volcanic field, as well as the eastern Snake River Plain and the Hebgen Lake, Lost River, and Teton late Quaternary normal faults. The GPS-derived velocities are compared to those of the Basin and Range province to interpret the kinematics of the YSRP in an intraplate tectonic framework. Strain rates for the Yellowstone Plateau were converted to moment rates and compared with moment release from earthquakes and fault slip to assess the deformation budget and estimate the relative contribution of seismic fault slip versus volcanic processes. Plausible processes contributing to deformation are discussed, including magma intrusion, fault slip, hydrothermal fluid pressurization, and postseismic viscoelastic relaxation.

2. Volcano-Tectonic Setting

[5] The widespread, bimodal silicic-basaltic volcanism associated with the Yellowstone–eastern Snake River Plain (YSRP) is thought to originate from an upper mantle plume based on recent tomographic imaging [e.g., *Waite et al.*, 2006; *Jordan et al.*, 2005; *Yuan and Dueker*, 2005]. During its 16-Myr history, a series of progressively younger silicic volcanic centers (each containing multiple calderas) developed along a 700-km-long track as the North America plate moved over the plume (Figure 1) from southwest Idaho to Yellowstone. The three most recent catastrophic eruptions occurred at 2.1 Ma, 1.2 Ma, and 0.64 Ma, forming the Yellowstone volcanic field [*Christiansen*, 2001].

[6] The youngest eruption produced the 60 km × 40 km Yellowstone caldera, where magmatic and tectonic activity continues with large earthquakes, earthquake swarms, rapidly changing patterns of ground motion, and extensive hydrothermal activity. Such activity distinguishes Yellowstone as a restless caldera [*Newhall and Dzurisin*, 1988].

[7] We refer the reader to other studies for a detailed account of the volcanic history, geology, and geophysics of the Yellowstone Plateau and eastern Snake River Plain [e.g., *Christiansen*, 2001; *Smith and Braile*, 1994; *Leeman*, 1982]. For this study, we summarize those tectonic and volcanic factors affecting YSRP deformation.

[8] Late Quaternary silicic volcanism is centered at the Yellowstone Plateau, located at the northeastern boundary of the Basin and Range province and the Rocky Mountain province (Figure 1). East-west extension of the Basin-Range accommodates much of the deformation of the western U.S. interior, with a total east-west opening rate of 12.5 mm/yr measured at the western Basin-Range, 1000 km southwest of Yellowstone [*Hammond and Thatcher*, 2004; *Thatcher et al.*, 1999]. South of Yellowstone at the Wasatch fault and the eastern Basin-Range boundary, the transition to the Rocky Mountain and Colorado Plateau provinces is marked by significant extension of 2 to 3 mm/yr [*Chang*, 2004], a shift of the effective elastic thickness of the lithosphere from 10 km to over 30 km [*Lowry and Smith*, 1995], and seismic activity [*Smith and Arabasz*, 1991]. Because the Yellowstone Plateau is located at the boundary of the Basin-Range and the Rocky Mountains, regional tectonic extension likely enhances volcanic deformation.

[9] Several prominent Basin-Range normal faults are adjacent to the Yellowstone Plateau and eastern Snake River Plain (Figure 1). These faults are capable of producing large, damaging earthquakes. In historic

time, the Hebgen Lake fault ruptured in the 1959 M7.5 Hebgen Lake, Montana, earthquake, and the Lost River fault ruptured in the 1983 M7.3 Borah Peak, Idaho, earthquake. Also of importance is the Teton fault, which has been historically quiescent but has had 30 m of offset in the last 14 kyr and Late Quaternary deformation rates of up to 2 mm/yr [*Byrd et al.*, 1994].

[10] Earthquakes are distributed in a parabolic pattern around the YSRP [*Smith and Arabasz*, 1991], and earthquake swarms are common at the Yellowstone Plateau [*Farrell et al.*, 2004]. Earthquake swarms have been interpreted to be related to heterogeneous stresses and are common in many active volcanic systems. For example, at the Long Valley caldera, California, earthquake swarms preceded uplift of the resurgent dome and were believed to result from fluid migration from the magma chamber [*Langbein*, 2003]. At Yellowstone, an earthquake swarm in 1985 coincided with the onset of caldera subsidence following decades of historic uplift [e.g., *Meertens and Smith*, 1991; *Waite and Smith*, 2002]. Another large swarm in 1999 coincided with the onset of renewed caldera subsidence.

[11] Most Yellowstone swarms and background seismicity are concentrated northwest of the Yellowstone caldera (Figure 1). This area, henceforth referred to as the northwest caldera boundary region, is associated with the northern boundary of the oldest 2.1 Ma caldera. In addition to frequent earthquakes, the region is notable for a series of north trending volcanic vents and hydrothermal basins associated with the East Gallatin–Reese Creek fault zone.

[12] A magmatic system of partial melt has been tomographically imaged beneath the axis of the Yellowstone caldera extending from depths of 8 to 16 km as well as a shallow hydrothermal CO_2 body northwest of the caldera [*Husen et al.*, 2004]. The shallow lobes of the magma system extend below the caldera's two resurgent domes: the 0.64 Ma Sour Creek dome to the northeast and the 0.16 Ma Mallard Lake dome to the southwest. This body is considered to be a crystallizing magma system that feeds Yellowstone's hydrothermal system. The injection of magma into this body and the accumulation and release of hydrothermal fluids (brines, gas, or magma) are considered highly plausible mechanisms for caldera deformation.

3. Deformation Measurement History

[13] The unprecedented historic deformation of the Yellowstone caldera was first identified by comparing data from leveling surveys between 1923 and 1977, revealing a total of 740 mm of caldera uplift [*Pelton and Smith*, 1982]. Subsequent leveling found different rates of uplift in the northeast and southwest caldera continuing through 1984 [*Dzurisin et al.*, 1990]. Caldera subsidence at 10 ± 20 mm/yr began in 1984–1985 and was first measured by early GPS campaigns [*Meertens and Smith*, 1991]. Interferometric synthetic aperture radar (InSAR) measurements between 1992 and 2003 revealed changing centers of subsidence and uplift in the northeast caldera, the southwest caldera, and northwest caldera boundary region [*Wicks et al.*, 1998, 2006].

[14] Following the 1959 M7.5 Hebgen Lake earthquake, high-precision leveling surveys were used to measure the vertical component of coseismic uplift and postseismic viscoelastic deformation [*Reilinger et al.*, 1977]. The leveling data revealed uplift in the epicentral region that preceded the earthquake and was not accounted for by viscoelastic relaxation. Later a trilateration network using electronic distance measurement methodology measured extension at 5.3 mm/yr for a 20-km baseline across the Hebgen Lake fault between 1973 and 1987 [*Savage et al.*, 1993].

[15] South of Yellowstone, geodetic evidence of contemporary deformation from six first-order leveling surveys across the Teton fault between 1988 and 2001 found episodes of unexpected hanging wall uplift at rates of up to 7 mm/yr [*Sylvester et al.*, 2001]. Paleoseismic studies of the Teton fault led *Byrd et al.* [1994] to extrapolate present-day extension rates of 0.1 to 0.2 mm/yr.

4. GPS-Measured Deformation

4.1. GPS Campaigns

[16] The Yellowstone–eastern Snake River Plain GPS data analyzed here were from seven field campaigns conducted over 16 years and from 15 permanent GPS stations that had been installed between 1996 and 2003 (Figure 2). The continuous data supplemented the campaign data in this study.

[17] The University of Utah and collaborators conducted the GPS campaigns in 1987, 1989, 1991, 1993, 1995, 2000, and 2003. During these surveys, field teams occupied 140 bench marks spanning a 200 by

300 km area of Yellowstone and the adjacent eastern Snake River Plain (SRP) (Table 1). Fifty of the stations were located in Yellowstone National Park, forty stations were located around the Hebgen Lake and Teton fault zones, and the remaining fifty stations were located in the eastern Snake River Plain and periphery of the YSRP.

[18] Base stations were established for the network and were run continuously during the periods of the campaign. At least two base stations were operated for each campaign prior to the establishment of the University of Utah continuous GPS network. GPS sites at the West Yellowstone airport, Montana, and at Lake Junction, Yellowstone, were used as base stations for 1987–1995. Baseline lengths ranged from less than 5 km to over 150 km. In 1995, a site in the eastern Snake River Plain was used as a base station, allowing shorter (<50 km) baselines for the other stations in the plain. Beginning in 2000, stations from the newly installed continuous GPS network were used as reference stations.

4.2. Continuous GPS Network

[19] Continuous GPS data acquisition began with the installation of the first station in the northeastern Yellowstone caldera in 1996 [*Chang, 2004*]. By 2003, the continuous network consisted of 15 stations, with four stations inside the caldera, two stations north of the caldera, two stations in the eastern Snake River Plain, one near the Tetons, and the remaining stations distributed outside the YSRP (Figure 2). Continuous stations were typically separated by distances of 100–150 km outside the Yellowstone Plateau and 12–50 km on the inside.

[20] The continuous stations used in this study had been operating at least 3 years. The station monuments were constructed using a concrete pillar design for long-term operations. Information on monumentation is available at http://facility.unavco.org/project_support/permanent/monumentation/monumentation.html. Positions were estimated daily for each site, providing good time resolution for tracking changes in position.

[21] The continuous GPS deformation data were compared with deformation trends determined from the campaigns. This was done in order to corroborate the campaign results, to observe transitions in deformation trends (i.e., from uplift to subsidence), and to identify short-term (<2 years) changes that the campaign GPS did not measure.

4.3. GPS Data Processing

[22] The campaign and continuous GPS data were processed with Bernese 4.2 processing software [*Rothacher and Mervart*, 1996]. Precise orbits from the International GPS Service were used for all campaigns after 1995. Earlier campaigns used orbits from the Defense Mapping Agency (DMA) and Scripps Institution of Oceanography (SIO). Although continuous GPS data were included in the campaign processing, the continuous GPS data were also processed separately to obtain position solutions [*Chang*, 2004].

[23] During the processing of each campaign, station positions were calculated relative to the base sites through differential GPS [e.g., *Hofmann-Wellenhof et al.*, 1992]. Base sites were located in the ITRF96 reference frame for the 1995, 2000, and 2003 campaigns and the continuous data by linking them to the International GPS Service (IGS) global network (see the auxiliary material). Because IGS data were not available for the older 1987–1993 campaigns, processing of these campaigns was done in a local reference frame.

[24] The daily position coordinates were combined to obtain a single campaign solution for each year. This was done by applying a Helmert transformation to bring the stations into the same reference frame and then solving for station positions through a weighted least squares adjustment [*Brockmann*, 1996].

[25] Site velocities were calculated by combining GPS data from multiple campaigns in a least squares algorithm using the ADDNEQ program [*Brockmann*, 1996]. The campaigns were sorted into three time windows to document changes in deformation over time. The time windows examined were 1987–1995, 1995–2000, and 2000–2003. The least squares estimation assumed linear deformation of each station during each time window.

[26] Velocities were determined in a fixed North America reference frame. This reference frame assumed no deformation in the stable continental interior, and velocities were relative to the interior. Stable North America was defined as the area to the east of and including the Rocky Mountain tectonic province.

[27] To constrain station velocities to a North America fixed reference frame, IGS stations were used as reference sites, and their velocities were constrained to the North America fixed velocities from *Bennett et al.* [2001]. In 1995–2000 and 2000–2003, IGS stations had their

coordinates and velocities constrained. For the 1987–1995 period, when IGS data were not available, three campaign sites distributed around the Yellowstone Plateau and were constrained to their 1995–2000 solution coordinates and velocities.

[28] The residuals between observed and calculated positions were plotted for both campaign and continuous GPS data. These plots, or time series, illustrated the change in position over time. Baseline time series were calculated for pairs of campaign sites by subtracting the motion of the second site with respect to the first, resulting in a record of relative motion between the sites. The campaign time series were placed in the auxiliary materials.

[29] In the case of continuous GPS data, station velocities were also calculated from a least squares estimation. Rather than using the combined network solutions, deformation rates were estimated directly from the time series. Velocities were calculated for short-term (<6 months) trends in ground motions at individual sites. The short-term velocities were included in the auxiliary materials.

4.4. Precision of GPS Determined Coordinates and Velocities

[30] The uncertainties associated with solutions for GPS positions and velocities were important for assessing and interpreting solutions and solution quality. We summarize the main sources of error, outline the steps we took to ensure reasonable error estimates, and compare our errors with published values for other campaigns.

[31] Numerous studies have analyzed GPS errors, and there has been a general consensus that formal errors of GPS position estimates are too low by a factor of at least 2 [e.g., *Hammond and Thatcher*, 2004; *Owen et al.*, 2000]. For example, daily formal errors for University of Utah permanent station positions are typically less than ±1 mm for the horizontal component. However, the day-to-day position solutions can vary by several millimeters, so that an uncertainty of ±3 to 5 mm is considered more appropriate.

[32] The precision of a solution can be determined from the amount of scatter or noise in a time series. Noise sources include instrument errors, satellite orbit errors, tropospheric modeling errors, monument instabilities, and reference frame errors [e.g., *Mao et al.*, 1999; *Williams et al.*, 2004; *Zhang et al.*, 1997]. The noise can be subdivided into time-dependent and time-independent sources.

[33] An evaluation of the GPS papers cited in this study showed that authors obtained errors for their GPS solutions by two principal methods: (1) estimation of noise in data based on models derived from spectral analysis or (2) root-mean-squares of residuals from a weighted least squares solution. We employed the second method to quantify the uncertainties of our position and velocity solutions. This method should include errors in the least squares estimate as well as observation errors and random (time-independent) noise.

[34] When combining daily solutions into a single campaign solution, weighting factors from station covariance matrices were applied to the normal equations to downweight outliers [*Brockmann*, 1996]. Campaign position errors were then calculated from the combination of individual station root-mean-square (RMS) values (Table 2) (see auxiliary material for individual station RMS values).

[35] GPS site velocities were calculated using least squares estimation. The least squares method was applied to each time window, to obtain three sets of velocities and velocity errors. The resulting horizontal RMS values were typically 0.2–1.5 mm/yr, while vertical values were ~6 mm/yr for most stations.

[36] To verify that the campaign RMS values computed for station positions and velocities were realistic, we compared them with results from other GPS campaign studies. The selected campaign example studies included the 1990–1996 Kilauea volcano project [*Owen et al.*, 2000], the 1992–2002 central Basin and Range project [*Hammond and Thatcher*, 2004], and the 1993–1995 Sierra Nevada project [*Dixon et al.*, 2000].

[37] For the Kilauea study, position coordinate errors were reported at ±2.5 to 10.8 mm for horizontal components and ±9.7 to 55.2 mm for the vertical components. The same study had horizontal velocity RMS errors from ±0.6 to 5.9 mm/yr and vertical errors of ±2.8 to 25.4 mm/yr. For the Basin-Range study, horizontal velocity RMS errors ranged from ±0.83 to 1.23 mm/yr. The Sierra Nevada study obtained horizontal RMS errors of ±0.5 to 2.7 mm/yr and vertical errors of ±2.7 to 5.8 mm/yr.

[38] The Yellowstone campaign position solutions had RMS values of ±1.4 to 11.7 mm in the horizontal and ±9.0 to 21.6 in the vertical, which were closely comparable to the Kilauea study. The Yellowstone

velocities had RMS values ranging from ±0.2 to 1.8 mm/yr for the horizontal and ±1.2 to 11.0 mm/yr for the vertical. Again, these values were comparable to the above studies.

[39] Errors for the continuously operating GPS sites were computed from the scatter in the time series. The goodness of fit was estimated by taking the RMS error of the difference between the fitted line and the observed values. The resulting RMS had average values of 2.0 mm/yr for the east component, 2.5 for the north component, and 5.5 for the vertical component.

5. Effects of Postseismic Viscoelastic Relaxation on Yellowstone–Snake River Plain Deformation

[40] Postseismic, time-dependent deformation from large earthquakes can contribute significantly to geodetically measured velocities. The Central Nevada Seismic Belt (CNSB) provides a good example of the effects of viscoelastic relaxation. GPS measurements between 1992 and 2002 found horizontal rates of 2 to 4 mm/yr, while InSAR measurements found range velocities of 2 to 3 mm/yr over a broad area that includes the Pleasant Valley, Dixie Valley, Fairview Peak, and Cedar Mountain fault zones. These geodetically measured velocities exceeded geologic slip rates of 0.5 to 1.3 mm/yr based on trenching studies of these fault zones. The discrepancy arose from viscoelastic deformation following several large, local earthquakes with magnitudes of 6.7 to 7.3 between 1915 and 1954 [*Gourmelen and Amelung*, 2005].

[41] In the YSRP, the 1959 M7.5 Hebgen Lake earthquake and 1983 M7.3 Borah Peak earthquake were the largest historic earthquakes in the study region. Several studies have measured postseismic relaxation of the Hebgen Lake earthquake, relying on leveling data to model lithospheric rheology beneath the fault zone [e.g., *Reilinger et al.*, 1977; *Holdahl and Dzurisin*, 1991; *Nishimura and Thatcher*, 2003].

[42] The most recent study by *Chang and Smith* [2006] applied the methodology of *Pollitz* [1997] to GPS data from this study and trilateration data from *Savage et al.* [1993]. The authors solved for rheologic parameters of an elastic upper crust overlying a viscoelastic lower crust and viscoelastic upper mantle half-space in the Hebgen Lake fault zone. The best fit model placed the bottom of the elastic upper crust at 18 ± 2 km and the bottom of the viscoelastic lower crust

at 31 ± 1 km. The viscosity of the lower crust was $3 \pm 2 \times 10^{21}$ Pa s, and the viscosity of the mantle was $2 \pm 1 \times 10^{19}$ Pa s.

[43] The rheology of the Lost River fault zone associated with the Borah Peak earthquake has not been modeled, due to the sparse geodetic data set for this fault zone. Postseismic leveling surveys, performed in 1984 and 1985 [*Stein and Barrientos*, 1985], were not sufficient for viscoelastic modeling. Since the Hebgen Lake and Lost River faults are both located in the extensional Basin-Range tectonic regime, we applied the rheologic model of *Chang and Smith* [2006] to the Lost River fault zone for a preliminary estimate of postseismic deformation from the Borah Peak earthquake.

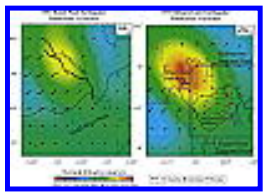

Figure 3. Velocity fields determined from modeling of viscoelastic relaxation following the 1959 M7.5 Hebgen Lake and 1983 M7.3 Borah Peak earthquakes. Vectors represent horizontal velocities, and color contours represent vertical velocities.

[44] The velocities arising from viscoelastic relaxation were calculated for both fault zones (Figure 3). For the Hebgen Lake fault zone, modeled horizontal velocities increased with distance from fault, attaining a maximum rate of approximately 1 mm/yr at distances of 20 to 40 km perpendicular to the fault trace. Predicted vertical velocities had a maximum rate of 2 mm/yr north of the fault scarp. For the Borah Peak region, average horizontal rates were 1 mm/yr near the Lost River fault. Maximum vertical rates were 1 mm/yr at the fault trace.

[45] Postseismic velocities were calculated for each time window: 1987–1995, 1995–2000, and 2000–2003. The viscoelastic component of the GPS-measured velocities was then removed by subtracting the modeled velocities from the observed velocities. Changes at most stations were less than 0.5 mm in the Hebgen Lake fault zone and less than 0.3 mm/yr in the Lost River fault zone (see auxiliary materials).

6. GPS-Measured Velocities

6.1. Yellowstone Caldera

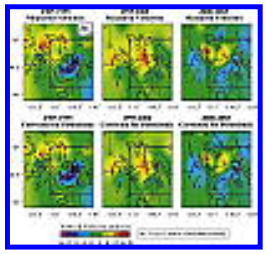

Figure 4. GPS-measured horizontal and vertical velocities of the Yellowstone Plateau at different time windows of 1987–1995, 1995–2000, and 2000–2003. Vectors represent horizontal velocities, and color contours represent vertical velocities. Error ellipses represent 1-σ uncertainties. (top) Observed velocities and (bottom) velocities corrected for viscoelastic relaxation.

[46] Ground motions of the Yellowstone Plateau were calculated for the three time windows of homogeneous crustal deformation, revealing secular changes in caldera motion (Figure 4). These data are summarized in Table 3.

[47] For 1987–1995, the caldera floor sank at a maximum rate of –14 ± 3 mm/yr near the Sour Creek dome for a total of 112 ± 24 mm. All stations near the central axis of the caldera subsided while stations on the caldera periphery moved radially inward at rates of 0.9 ± 0.3 to 7.3 ± 0.5 mm/yr.

[48] For the period 1995–2000, the caldera returned to uplift, but maximum uplift was concentrated to the northwest of the caldera in the northwest caldera boundary region. The maximum rate there was 15 ± 4 mm/yr for a total of 75 ± 20 mm. This deformation was accompanied by a radial pattern of horizontal motion directed away from the uplift center at rates up to 6.7 ± 0.6 mm/yr, indicating inflation.

[49] In 2000–2003, uplift continued in the northwest caldera boundary region at 12 ± 4 mm/yr for an additional 36 ± 12 mm of displacement, while subsidence resumed in the central caldera axis at a maximum rate of –9 ± 6 mm/yr for an additional 27 ± 18 mm subsidence. As in the previous time periods, the horizontal motion vectors were pointed away from the uplift center and directed inward toward the subsidence axis. Horizontal rates were similar to those of prior time windows, ranging from 0.3 ± 0.5 to 7.4 ± 0.5 mm/yr. These rapid temporal changes suggest a key result of this study, namely that the Yellowstone caldera behaves with rapid variations of uplift to subsidence over decadal periods.

[50] On a larger scale, the southwest Yellowstone Plateau moved to the southwest at all time periods (Table 3). Average rates in this region,

calculated from stations in the western caldera and near the western park boundary, were 2.2 ± 0.2 mm/yr in 1987–1995, 4.3 ± 0.2 mm/yr in 1995–2000, and 4.1 ± 0.2 mm/yr in 2000–2003. The low extension rate for 1987–1995 was thought to be influenced by subsidence within the caldera, with its inward directed horizontal motions. The higher extension rates after 1995 would then have been influenced by inflation in the Yellowstone Plateau. We believe that these observations show the influence of regional lithospheric extension associated with the Late Quaternary opening of the eastern Basin-Range province.

6.2. Hebgen Lake Fault

[51] West of the Yellowstone caldera, notable crustal extension was observed across the Hebgen Lake fault even after viscoelastic corrections were applied (Figure 4). On the footwall (north) side of the south dipping fault, stations moved to the northeast at rates of 1.0 ± 0.5 to 3 ± 1 mm/yr. On the hanging wall to the south, stations moved south and west at rates of 0.8 ± 0.4 to 4 ± 2 mm/yr.

[52] All sites experienced net uplift from 1987 to 2003. Of this uplift, postseismic viscoelastic deformation contributed up to 30 mm to the total uplift. When the viscoelastic component was subtracted from site velocities and station time series, significant uplift remained. Uplift rates (after viscoelastic corrections) within 15 km of the fault generally ranged from 4 ± 3 to 11 ± 2 mm/yr, with some outliers of 16 ± 5 to 18 ± 7 mm/yr.

[53] All baselines across the Hebgen Lake fault increased in length, indicating dominant crustal extension (see auxiliary material). Average horizontal extension rates were calculated from the three baselines crossing the fault for each time window. The average extension rates varied from 3.1 mm/yr in 1987–1995 to 5.3 mm/yr in 1995–2000 and 4.2 mm/yr in 2000–2003 (Table 3). Uncertainties for the baseline extension rates were not computed because the 1995–2000 and 2000–2003 time windows each had only two points, precluding estimation of scatter.

[54] *Chang and Smith* [2006] used the baseline data from this study in the modeling of the viscoelastic relaxation. Therefore the baselines have not been adjusted for viscoelastic effects and would have higher extension rates as a result.

[55] As noted previously, postseismic viscoelastic relaxation

corrections were subtracted from the total station velocities. Viscoelastic effects accounted for 15–20% to the uplift and up to 20% of the extension in the Hebgen Lake fault zone and northwest caldera boundary region. For example, a site within 5 km of the fault was recorded to have uplift of 149 ± 34 mm of uplift between 1987 and 2003. After corrections for viscoelastic relaxation were applied, the uplift was fount to be 119 ± 34 mm, a difference of 20%.

6.3. Teton Fault

Figure 5. Horizontal (black) and vertical (white) velocities measured in the Teton fault network from 1987 to 2003. Two sites on the Teton mountain block were fixed to estimate velocities in a local reference frame. Error ellipses represent 1-σ uncertainties.

[56] South of the Yellowstone caldera, GPS data were used to evaluate deformation of the adjacent Teton fault. To eliminate the possibility that eastward aseismic slip on the fault was obscured by regional westward motion of the Yellowstone Plateau, site velocities in the Teton region were recomputed in a local reference frame defined by holding two footwall stations on the Teton mountain block fixed (Figure 5).

[57] Despite the reference frame adjustment, deformation in the Teton region was not consistent with expected normal fault loading. Valley (hanging wall) sites moved westward at an average rate of 0.34 ± 0.06 mm/yr between 1987 and 2003. At the same time, the hanging wall uplifted at an average rate of 2.4 ± 0.5 mm/yr.

[58] Precision leveling measurements of an east-west line of bench marks perpendicular to the Teton fault discovered uplift on the hanging wall of the Teton fault between 1988 and 2001 [*Byrd*, 1995; *Sylvester et al.*, 2001]. Most of the leveling-measured hanging wall uplift was within 2 km of the fault trace, with deformation rates varying from 7 mm/yr uplift to 6–8 mm/yr subsidence, but with a net uplift.

[59] A study of postglacial (<14 ka) surface offset revealed Teton vertical fault slip rates of 0.1 to 0.2 mm/yr for the past 5000–7000 years [*Byrd*, 1995]. The low slip rate was less than the uncertainties of the GPS velocities and so would not have been accurately measured by the GPS campaigns. Therefore we rule out tectonic slip as the primary

deformation mechanism in the Teton fault zone.

6.4. Eastern Snake River Plain and Surrounding Basin-Range Tectonic System

Figure 6. GPS-measured eastern Snake River Plain horizontal velocities for the time period 1995–2000. Error ellipses represent 1-σ uncertainties.

[60] Deformation of the eastern Snake River Plain (SRP) and surrounding Basin-Range faults was derived from the 1995 and 2000 campaigns. Horizontal ground motions of sites in the SRP were generally in the southwest direction relative to stable North America (Figure 6).

[61] The average velocity of the SRP was 2.1 ± 0.2 mm/yr with an azimuth of 191° parallel to the axis of the plain, as calculated from sites between 112° and 114°W and inside the SRP (Table 3). This was less than the 4.3 ± 0.2 mm/yr extension across the caldera during the same time period, so there must have been contraction between the Yellowstone Plateau and SRP. Many of the stations along the northern boundary of the SRP had a component of southward motion, while stations in the southern part of the plain showed southwest to westward motion, suggesting axial contraction along the length of the plain (Figure 6).

[62] The adjacent Basin-Range regions to the north and south of the plain in Idaho Basin-Range fault province had comparable velocities to the stations within the plain (Figure 6). The average velocity of GPS stations north of the SRP was 2.0 ± 0.4 mm/yr at an azimuth of 217°. The two sites south of the plain (excluding stations in the Rocky Mountains) had an average velocity of 3.4 ± 0.7 mm/yr at an azimuth of 241°. Although this velocity was greater than the southwest motion for the SRP, it was dominated by a high rate of 5.3 ± 0.9 mm/yr measured at one of the two sites. The azimuth of 241° for the Basin-Range, when compared to the azimuth of 191° for the SRP, requires contraction between the two provinces. This may be accommodated by axial contraction in the SRP.

[63] Several large normal faults abut the SRP (Figure 1). To the north, the Beaverhead fault, Lemhi fault, and Lost River fault have a combined horizontal motion of 2 mm/yr, while to the south the only fault with reported horizontal slip rates greater than 0.2 was the Grand Valley fault, with 0.5 mm/yr [*Machette et al.*, 2001].

[64] The effects of postseismic relaxation were minor: less than 0.3 mm/yr in the Lost River fault zone. Within the Snake River Plain, modeled postseismic velocities were less than 0.1 mm/yr and did not change the measured velocities.

6.5. Comparison of Campaign and Continuous GPS Velocities

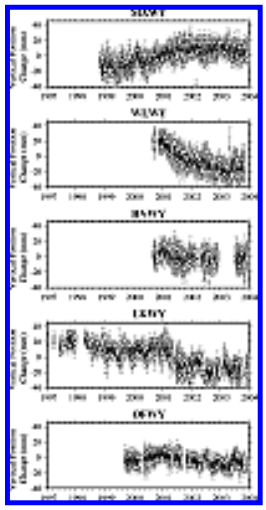

Figure 7. Time series of vertical components of continuous GPS stations in the Yellowstone Plateau. Increasing displacements over time indicate uplift; decreasing displacements indicate subsidence. Error bars are obtained from weighted RMS of daily solutions.

[65] Trends of Yellowstone caldera uplift and subsidence identified from the campaign GPS were compared with trends identified from the continuous GPS time series (Figure 7). We note that the campaign GPS measured net deformation between campaigns, while the continuous GPS measured daily deformation and allowed the identification of short-term changes in position that occurred over periods of weeks to months.

[66] For 1995–2000 we examined station LKWY (Figures 2 and 7) in the northeast caldera, which has operated since mid-1997 and is the longest operating continuous GPS site in Yellowstone. This station had net subsidence, <10 mm, between 1997 and 2000. Net uplift at the nearest campaign stations was 20–25 mm, suggesting a possible episode of rapid uplift in the northeast caldera between late 1995 and 1997 to account for the discrepancy. This was confirmed by Yellowstone InSAR measurements, which found 15 mm of uplift in this area between 1995 and 1997 [*Wicks et al.*, 1998].

[67] For 2000–2003, campaign GPS measurements found caldera subsidence of −9 ± 6 mm/yr and northwest caldera boundary uplift of 12 ± 4 mm/yr. The northeast caldera site LKWY had a period of rapid subsidence of −45 ± 6 mm/yr from 2001.0 to 2001.8, with no additional net deformation through 2003. The total 2001 subsidence for LKWY was about 36 mm, the same as the 36 mm calculated for total 2000–2003 period from the campaign GPS measurements. Two other stations in the northeast caldera (HVWY and WLWY) also experienced net subsidence between 2001 and 2003, with most subsidence occurring in 2001. The southeast caldera station at Old Faithful (OFWY) rose and subsided through 2003 but had no net deformation (Figure 4), probably due to its location outside the main region of subsidence. The station at Mammoth (MAWY) had uplift from 2000 to 2003 that shifted to subsidence in 2003.

[68] A continuous GPS station in the eastern Snake River Plain (GTRG) and an adjacent station north of the Snake River Plain (AHID) experienced southwest horizontal motion of 3 ± 2 mm/yr for 1998–2003, which was similar to the average campaign-determined velocity of 2.1 ± 0.2 mm/yr for 1995–2000.

[69] The campaign and continuous GPS measurements thus agreed on the net deformation directions and rates of the Yellowstone Plateau and Snake River Plain. In addition, the continuous GPS data revealed fluctuations in caldera ground motion over periods of months that we attributed to active volcanic processes. These fluctuations included the 2001 episode of subsidence in the northeast caldera and the probable 1995–1997 uplift in the same region. Overall, the continuous GPS data indicate that most deformation occurred in shorter episodes lasting 6–12 months.

7. Velocity and Strain Rate Fields

[70] The GPS-derived velocity and strain rate fields were calculated for the Yellowstone caldera and adjacent regions using the interpolation algorithm of *Shen et al.* [1996]. The corresponding principal strain rates and dilatation rates were calculated and represented the change in velocity over space and the volumetric changes accompanying the deformation, respectively.

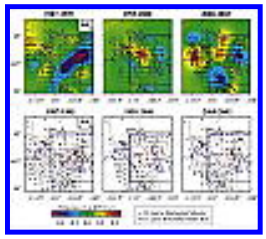

Figure 8. (top) Principal strain rates and (bottom) horizontal velocity fields for each of the three time windows of Figure 4. Strain rates are plotted as crosses and show direction of deformation. Dilatation rates representing fractional volume changes are shown as color contours in Figure 8 (top).

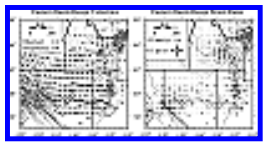

Figure 9. (left) Horizontal velocity field and (right) principal strain rates for the eastern Basin and Range province and the YSRP determined by GPS measurements.

[71] Velocity and strain rate fields were estimated for the YSRP at local and regional scales. On the local scale, Yellowstone Plateau deformation was interpolated at a grid spacing of 0.1° for each of the three time windows (Figure 8). At the regional scale, the YSRP GPS velocities were combined with velocities from *Bennett et al.* [2003], *Thatcher et al.* [1999], *Chang* [2004], and the University of Utah GPS network to determine the velocity field for the YSRP and the northern Basin-Range on a 0.5° grid (Figure 9).

[72] The magnitudes and orientation of the average principal strains for different regions of the Yellowstone Plateau and SRP are given in Table 4. The dilatation rate, or fractional volume change rate Δ, was also derived from the principal strains and reflected the episodes of inflation/deflation and extension/contraction.

[73] At the Yellowstone Plateau, contractional strains were associated with subsidence and extensional strains were associated with uplift of the caldera. Dilatation rates were negative in areas of subsidence and positive in areas of uplift (Figure 8). In 2000–2003, two centers of subsidence were observed at the northeast and southwest caldera boundaries. The subsidence affected the velocity and strain fields as far south as the southern Yellowstone park boundary.

[74] In the Hebgen Lake fault zone, the horizontal principal strains were oriented perpendicular to the fault and implied fault-normal extension. The strain rates ranged from 0.15 ± 0.02 to 0.18 ± 0.03 $\mu\varepsilon$/yr, corresponding to extension of 3.0 to 3.6 mm/yr for a 20-km-wide fault zone. These rates differed from the 3.1 to 5.3 mm/yr derived from baseline length changes, but the baselines would have included a

contribution from the northwest caldera boundary uplift associated with postseismic viscoelastic deformation. The high strain rate of 0.18 ± 0.03 $\mu\varepsilon$/yr coincided with inflation in the northwest caldera boundary region in 1995–2000 (Table 4).

[75] The YSRP displacement and strain rate fields reflected the rotation of extension directions around the Yellowstone caldera and the general southwest motion of the SRP in 1995–2000 (Figure 9). Velocities north of the SRP were directed to the south, while velocities to the south were oriented to the west. Because of this, the strain rates showed contraction perpendicular to the long axis of the YSRP.

[76] Snake River Plain strain rates were generally low (<0.01 $\mu\varepsilon$/yr) when compared with the Yellowstone Plateau, with contraction inferred for the northeast SRP arising from rapid extension at the Yellowstone Plateau and slower motion in the SRP. The low strain rates indicated little deformation within the SRP.

[77] Another study of the eastern Snake River Plain incorporated some of our GPS data to measure deformation between 1995 and 2004 [*Rodgers et al.*, 2005]. The authors found no significant internal deformation of the SRP and concluded that it behaves as a rigid block, in contrast to our results of some internal contraction. They obtained southwest SRP motion of 2.8 ± 0.3 mm/yr, which was larger than our rate of 2.1 ± 0.2 mm/yr by a 130%.

[78] Strain rates were averaged and compared for the Lost River fault zone and adjacent portions of the Snake River Plain (Table 4). The maximum principal strain rates were similar: 0.04 ± 0.01 $\mu\varepsilon$/yr north of the SRP and 0.03 ± 0.02 $\mu\varepsilon$/yr within the SRP. Although strain rates were similar inside and outside the SRP, there was rotation in the strain axes orientations (Figure 9).

8. Comparison of Seismic, Geodetic, and Geologic Moments

[79] Deformation mechanisms can be divided into seismic and aseismic sources. Seismic sources consist of fault slip during earthquakes, while aseismic sources include elastic loading, postseismic viscoelastic relaxation, and volcanic inflation and deflation.

[80] To assess the contribution of different deformation sources, the

total (geodetic), seismic, and geologic moments were calculated and compared for the Yellowstone Plateau. The conversion of strain rates, earthquake magnitudes, and fault slip rates to moments allowed the comparison of geodetic deformation with elastic deformation from earthquakes and regional geologic data. This comparison followed the method described by *Ward* [1997].

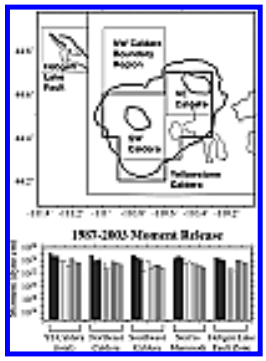

Figure 10. (bottom) Histogram of geodetic (dark gray), seismic (white), and geologic (light gray) moments for different regions in the Yellowstone Plateau. The three bars for each moment type represent the three time windows of 1987–1995, 1995–2000, and 2000–2003. (top) Map showing different regions of the plateau, with the caldera area outlined in bold.

[81] Total (geodetic) moments were calculated from the maximum principal strains for each time period using Kostrov's formula [*Kostrov*, 1974]. Strain values were obtained by multiplying the strain rates from the previous section by years of observation, and the seismogenic thickness [*Smith and Arabasz*, 1991] was set to 10 km. Gridded values were summed to obtain the total moments for the Yellowstone caldera, the northwest caldera boundary region, and the Hebgen Lake fault zone (Figure 10).

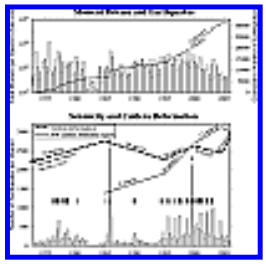

Figure 11. Plot of Yellowstone Plateau seismicity, deformation, and moment release. (top) Histogram showing the moment release per quarter and the cumulative number of earthquakes. (bottom) Histogram showing number of earthquakes per quarter and trends in caldera deformation from leveling and GPS campaigns. Earthquake swarms are marked by arrows.

[82] The seismic moment was calculated from the magnitudes of earthquakes from the Yellowstone catalog [*Husen and Smith*, 2004]. An empirical relation that was developed explicitly for extensional regime normal-faulting earthquakes was used to convert earthquake magnitude to moment [*Doser and Smith*, 1982]:

$$\log M_{seis} = 1.1\,M + 18.4$$

where M_{seis} was seismic moment in dyne centimeters and M was earthquake magnitude. The resulting moment data were sorted by time period and location and summed to obtain total seismic moments for the same regions as the geodetic data (Figure 10). The moment data were additionally sorted by time to obtain moment release in the Yellowstone Plateau per quarter year (Figure 11).

[83] For the geologic moment, fault slip rates for major faults in Yellowstone Plateau were obtained from *Wong et al.* [2000]. Horizontal slip components were calculated assuming a fault dip of 60°. The horizontal slips were then converted to strain rates assuming a fault zone width of 20 km, and strain rates were converted to moment release during each time period. We used slip rates from the Hebgen Lake fault, the East Gallatin–Reese Creek fault for the northwest caldera boundary region, the Mallard Lake fault zone for the southwest caldera, and the Mirror Plateau fault zone, Buffalo fault, and Sour Creek fault zone for the northeast caldera.

[84] The total and seismic moments are compared in Figure 10, revealing that the geodetic moment exceeded the seismic moment by at least 1 order of magnitude in all areas. The greatest total moment was in the Yellowstone caldera, with values of 10^{24} to 10^{25} dyn cm, which is equivalent to a M5–6 earthquake during every time period. The seismic moment for the caldera was on the order of 10^{23} dyn cm, which is equivalent to a M4.2 earthquake for each period. In the northwest caldera boundary region, total moments were 10^{24} dyn cm and exceeded the seismic moment by only 1 order of magnitude. This was attributed to the higher rates of seismicity in this region.

[85] The total moment in the Hebgen lake fault zone was 10^{24} dyn cm, 2 orders of magnitude greater than the seismic moment. It has been noted that background seismicity of the Hebgen Lake fault is low compared to the Yellowstone Plateau, and that there have been little significant aftershock activity since the 1959 event. The 1959 earthquake was not included in the moment calculations because it predated the establishment of both seismic and GPS networks in the park. Had the estimated moment release of 10^{27} dyn cm [*Doser*, 1985] been included in the cumulative seismic moment, then there would have been no discrepancy between total and seismic moment release.

[86] *Ward* [1997] noted that rapidly deforming faults with frequent,

large earthquakes, such as the San Andreas fault, have nearly equal seismic and total moment rates, while more slowly deforming regions such as the YSRP and eastern Basin-Range have much larger total moment rates than seismic moment rates, and require long monitoring periods to record a reliable estimate of earthquake rates. Therefore we used Late Quaternary fault slip rates to estimate the long-term geologic moment release (Figure 10).

[87] The total geologic moments for each region ranged from 10^{22} to 10^{24} dyn cm, with the Yellowstone caldera having the highest moments. The Hebgen Lake fault zone also revealed large geologic moments of 10^{23} to 10^{24} dyn cm, within 1 order of magnitude of the total moment release. In the Yellowstone caldera, geologic moment rates exceeded seismic moment rates by 1 order of magnitude in 1995–2000, except in the southwest caldera. In the northwest caldera boundary region, seismic moment slightly exceeded geologic moment.

[88] The presence of unidentified faults could lead to discrepancies between M_{tot} and M_{geol} [*Ward*, 1997]. Because M_{tot} and M_{geol} in the Yellowstone caldera have similar values, there are likely few or no additional major faults contributing significantly to deformation, and the geodetically measured ground motions can be inferred to be associated with the faults of the resurgent domes, the Mirror Plateau fault zone, and the Buffalo Fork fault. In the northwest caldera boundary region, M_{tot} exceeded M_{geol}, so the East Gallatin–Reese Creek fault zone was not the sole source of deformation.

[89] Aseismic volcanic inflation or deflation, which contributes to neither M_{geol} nor M_{seis}, must also be considered in the deformation budget and is likely to add to the discrepancies between the total moment and the seismic and geologic moment.

[90] When seismic moment release over time was examined (Figure 11), the greatest moment release was associated with the 1975 Norris Junction earthquake. The amount of seismic moment fluctuated by 3–4 orders of magnitude but did not obviously follow any of the trends of caldera deformation. While there was no sustained moment release associated with uplift or subsidence, large swarms coincided with transitions from uplift to subsidence in the caldera in 1985 and 1999. However, these swarms released 10^{24} dyn cm of moment, which was consistent with the background moment release range of 10^{23} to 10^{24} dyn cm.

9. Discussion

9.1. Yellowstone Volcanism and Caldera Deformation

[91] Caldera uplift and subsidence trends are common in active volcanic systems. Such deformation has been associated magmatic processes: the injection and migration of magma, and the cooling and crystallization of magma. Depending on magma composition and crustal conditions, the crystallizing magma may release water and other volatiles that may be trapped in overpressured zones and cause uplift, or that may escape into the crust and cause subsidence. Cooling and contraction of magma with no water can also cause subsidence.

[92] Deformation of the Yellowstone caldera was compared to the Long Valley caldera at Mammoth Lakes, California, where recent activity was due to magma injection. Our data were also compared with the Campi Flegrei caldera, a volcano in Italy where recent deformation was linked to hydrothermal processes.

[93] Long Valley caldera's unrest episodes have been linked to the migration of magma beneath its resurgent dome [*Langbein*, 2003]. In the deformation episodes, resurgent dome uplift either preceded or was contemporaneous with earthquake swarm activity about 5 km to the south. Most earthquakes were tectonic in origin, but some earthquakes had long-period frequency spectra consistent with magmatic sources [*Pitt and Hill*, 1994]. Results from gravity measurements between 1982 and 1998 were consistent with the intrusion of rhyolitic magma into the upper crust [*Battaglia et al.*, 1999].

[94] When contrasted with Long Valley unrest, Yellowstone caldera deformation was generally less rapid when measured over a period of years by the Yellowstone campaign data (Table 5). Although continuous data only became available after 1996, short periods of more rapid deformation were recorded that may resemble Long Valley unrest. While the maximum uplift rate for Long Valley was 100 mm/yr [*Langbein*, 2003], the maximum Yellowstone caldera uplift 62 ± 6 mm/yr for a 4-month period in 1999.

[95] Long Valley unrest has been clearly associated with earthquake swarms [e.g., *Langbein*, 2003], but the correlation was not as clear at Yellowstone (Figure 11). Significant earthquake swarms did coincide with changes from uplift to subsidence, but the number of swarms

greatly exceeded the number of changes in deformation.

[96] At the Campi Flegrei in Italy, modeling of leveling, trilateration, and gravity data have notably confirmed that recent episodes of unrest were caused by hydrothermal fluid migration rather than magma intrusion [*Battaglia et al.*, 2006]. Unrest at Campi Flegrei consisted of 1.8 m of uplift from 1982 to 1984, which was equivalent to 900 mm/yr (Table 5), and which was more rapid than even maximum Long Valley uplift of 100 mm/yr. The uplift was followed by subsidence at an average rate of 50 mm/yr through 1995.

[97] When *Battaglia et al.* [2006] modeled source geometry and density, they found the best fit sources had shallow (<4 km) depths and densities on the order of 1000 kg/m^3. These results were consistent with a hydrothermal fluid source. A magmatic source would have had a density of at least 2500 kg/m^3. The authors favored a model of accumulation and release of hydrothermal fluids from overpressured reservoirs similar to that described by *Fournier and Pitt* [1985] and other studies. The results from this study demonstrated that such a mechanism could produce rapid and large deformation. Additionally, *Battaglia et al.* [2006] suggested that hydrothermal pressurization might have been triggered by magma intrusion.

[98] At Yellowstone, magma migration is required to maintain the very high heat flow and hydrothermal activity but is not necessary for short-term deformation. Moreover, no deep, long-period earthquakes have been observed at Yellowstone to confirm magma migration.

[99] Precision time-dependent gravity surveys have measured mass changes in the Yellowstone caldera consistent with magma intrusions in 1977–1983 but found no mass changes during 1986–1993, when the caldera floor was subsiding [*Arnet et al.*, 1997]. No gravity data were available for the 1995–2000 caldera uplift, so magma intrusion cannot be ruled out.

[100] An alternative to magma intrusion is pressurization of a deep hydrothermal system. The brittle-ductile transition acts as a barrier to fluid flow [*Fournier and Pitt*, 1985] and occurs at depths as shallow as 5 km in the Yellowstone caldera [*Smith and Arabasz*, 1991]. As rhyolite in the magma chamber crystallizes, brines are released but trapped below the brittle-ductile transition, leading to increased pressure and inflation. This mechanism has no net change in mass and should cause

no changes in the gravity field during caldera uplift [*Arnet et al.*, 1997].

[101] Depressurization of the deep hydrothermal system causes subsidence as fluids escape. After a period of uplift, the overpressured zone is breached due to hydrofracturing, an earthquake, or magma intrusion [*Fournier*, 1999]. The previously trapped brines escape and the reservoir deflates. This may have happened during the 1985 swarm just prior to the beginning of subsidence [*Waite and Smith*, 2002]. The escape of fluids from the caldera to the northwest may have contributed to uplift in the northwest caldera boundary region.

[102] It should be noted that swarms and earthquakes in Yellowstone are not necessarily due to the same underlying mechanism of fluid migration as the deformation. Rather, they may be triggered by changes in the stress field arising from the deformation.

9.2. Regional Deformation of the YSRP and Basin and Range

Figure 12. Summary map of GPS-measured deformation vectors derived from this study for the YSRP. Average GPS rates are labeled in large font. Fault slip rates from *Byrd et al.* [1994], *Haller et al.* [2002], and *Wong et al.* [2000] were converted to horizontal extension rates assuming a fault dip of 60° and are labeled in small fonts. For comparison, minimum principal stress indicators from other studies are also shown. T axis directions are from *Waite* [1999], focal mechanisms and vent alignments are from *Zoback* [1992], moment tensor solutions are from http://quakes.oce.orst.edu/moment-tensor, and mapped rift zones are from *Smith et al.* [1996].

[103] We combined the Yellowstone–Snake River Plain GPS data with Basin-Range data to obtain regional deformation patterns of the western U.S. interior (Figure 9). The southwest motion of the YSRP rotated to westward motion in the Basin-Range (Figures 9 and 12). There was little to no deformation in the Rocky Mountains, and extension dominated at the eastern Basin-Range and Yellowstone Plateau.

[104] The GPS-derived velocity field was consistent with the microplate model for western U.S. deformation, with deformation concentrated at microplate boundaries [*McCaffrey*, 2005]. The tectonic provinces of the western United States correspond to microplates that accommodate relative motion between the North America plate and Pacific plate. *McCaffrey* [2005] modeled lithospheric blocks of the southwest United States and treated the eastern Basin and Range as a separate block. Our results indicate that the eastern Snake River Plain is also an independent microplate of western North America.

[105] Southwest motion across the Yellowstone Plateau was interpreted to accommodate a significant component of Basin-Range regional extension. Yellowstone extension ranged from 2.2 ± 0.2 mm/yr in 1987–1995 to 4.1 ± 0.2 mm/yr in 2000–2003. In contrast, the northern Wasatch fault was determined to have 2.7 ± 1.3 mm/yr extension [*Martinez et al.*, 1998; *Chang and Smith*, 2006], while the southern Wasatch fault had 1.3 ± 0.5 mm/yr extension [*Hammond and Thatcher*, 2004].

[106] The higher extension rates at the Yellowstone Plateau relative to the Wasatch fault are the result of active volcanic processes of the Yellowstone caldera. These processes include caldera inflation/deflation and thermally enhanced stretching of the crust. High heat flow associated with the magma chamber has thinned the brittle crust so that the brittle-ductile transition is as shallow as 5 km depth in the caldera versus 12–15 km outside the caldera. This high thermal flux was also predicted to reduce the viscosity of the lower crust and upper mantle, which would affect the rate and the amount of deformation in response to an applied stress.

10. Concluding Remarks

[107] This paper summarized a 16-year study of lithospheric deformation of the Yellowstone–Snake River Plain volcanic field and the surrounding northern Basin-Range province from 7 GPS campaigns and 15 continuous GPS sites. The campaign data revealed variable styles and rates of deformation, with extension dominating at the regional scale and local vertical perturbations at the Yellowstone Plateau. Postseismic viscoelastic relaxation also contributed to deformation of the Hebgen Lake fault and extended into the northwest caldera boundary region.

[108] The continuous GPS data show that the rates of vertical motion

at the caldera were not uniform, but fluctuated from uplift to subsidence over periods of months. For the northeast caldera, most of the subsidence between 2000 and 2003 occurred in 2001. The campaign and continuous GPS sites both showed different rates for the northeast and southwest caldera.

[109] We favor a model of pressurization of the deep hydrothermal-magmatic system as the dominant deformation mechanism during the 16-year study period. In this model, escape of brines from a deeper magma reservoir led to caldera subsidence in 1987–1995 and 2000–2003. Escaping fluids flowed to the northwest, where they likely contributed to uplift in the northwest caldera boundary region.

[110] A comparison of seismic and geodetic moment rates of the Yellowstone Plateau revealed that total deformation exceeded tectonic deformation (as estimated by seismic and geologic moments) by 1–2 orders of magnitude (Figure 10). Discrepancies between total, seismic, and geologic moments were attributed to a combination of aseismic processes, including volcanic inflation and deflation and postseismic viscoelastic relaxation. Most seismic moment is released in large earthquakes, so the absence of such large (M6–7) earthquakes in 1987–2003 contributed to the deficit of seismic moment.

[111] Declining extension rates across the Hebgen Lake fault zone between 1973–1987 and 1987–2003 support the model of significant postseismic viscoelastic relaxation following the 1959 Hebgen Lake earthquake. The postseismic viscoelastic effects did not account for all the observed extension and uplift at the fault zone but were still a significant component of deformation near the fault. Uplift at the northwest caldera boundary region likely contributed to Hebgen Lake deformation. At the same time, viscoelastic deformation also contributed to the northwest caldera boundary region uplift at rates of 1 to 2 mm/yr.

[112] For the Teton fault, no evidence was noted for expected eastward normal fault extension (Figure 5). Instead, the hanging wall was found to have a component of westward directed ground motion, so that there was contraction on the fault. This unusual deformation was accompanied by uplift in the valley of Jackson Hole.

[113] The eastern Snake River Plain was found to be moving southwest at an average rate of 2.1 ± 0.2 mm/yr (Figure 12). When compared with campaign and continuous site velocities in adjacent

portions of the Basin and Range, the velocities were the same within measurement errors, though the average direction of motion varied. Westward motion of the Basin-Range may contribute to axial contraction in the SRP.

[114] In contrast to the SRP motion, the Yellowstone Plateau deformation included a strong component of southwest extension at up to 4.3 ± 0.2 mm/yr in 1995–2000. Yellowstone extension rates were correlated with caldera deformation, with the highest rate during a period of caldera uplift. The Yellowstone extension rates greatly exceeded the southwest motion of the SRP in 1995–2000, suggesting contraction at the transition between the two regions during periods of uplift in the Yellowstone Plateau.

[115] We note that beginning in 2004, the northeast Yellowstone caldera began to rise at rates of up to 60 mm/yr (Figure 11), and that this deformation has continued into mid 2006 [*Smith et al.*, 2005]. At the same time, subsidence was initiated in the northwest caldera boundary region. No earthquake swarms had occurred between 2004 and the end of 2005.

Acknowledgments

[116] The University of Utah (UU) collaborated with UNAVCO, Yellowstone and Grand Teton National Parks, Idaho National Laboratory (INL), Brigham Young University (BYU), and U.S. Geological Survey (USGS). Rob Reilinger collaborated with us on the 1987 and 1989 projects and allowed us use of the GPS campaign data from his MIT group. The National Geodetic Survey participated in the 1987 surveys and established several new GPS bench marks in the Yellowstone area. Rick Hutchinson of the National Park Service materially assisted with the early Yellowstone GPS campaigns. Dan Dzurisin collaborated with us on installation of two of the permanent GPS stations in Yellowstone. Ron Harris of BYU and students assisted with field GPS surveys in Idaho. Suzette Payne of the Idaho National Laboratory was instrumental with GPS surveys and the operation of a continuous GPS station in the Snake River Plain. David Rodgers of Idaho State University contributed results from his own Snake River Plain GPS work for comparison with our data. A complete list of participants and organizations that worked on this project is included in Text S1 in the auxiliary material. We would like to thank these institutions for their contributions of personnel, equipment, expertise, and site access. Specifically, the University of Utah and the University

of Utah Seismograph Stations provided computational and technical support, and UNAVCO provided instrument and technical support. Special thanks also go to Michael Jordan, who provided useful criticism of this paper, and John Braun, who gave helpful advice and instructions on the velocity calculation program. Theresa Van Hove of UCAR and UNAVCO archived the GPS data and contributed to the field work and processing. Tony Lowry of the University of Utah has been a long-time associate and contributor to the GPS field work. Richard Snay at NGS was most helpful with initial strain analysis. Zheng-Kang Shen (UCLA) provided algorithms for the strain analysis. This paper benefited from the useful and constructive reviews of Robert Reilinger and an anonymous reviewer. The project was part of a larger study titled “Geodynamics of the Yellowstone Hot spot by Seismic and GPS Imaging” and was supported by the National Science Foundation, Continental Dynamics and Earth Science programs, grants 0314298, 9725431, and 9316289.

Citation: Puskas, C. M., R. B. Smith, C. M. Meertens, and W. L. Chang (2007), Crustal deformation of the Yellowstone–Snake River Plain volcano-tectonic system: Campaign and continuous GPS observations, 1987–2004, *J. Geophys. Res.*, *112*, B03401, doi:10.1029/2006JB004325.